Synergism of Electrochemical and Mechanical Factors in Erosion−Corrosion

B. T. Lu and J. L. Luo*

Department of Chemical and Materials Engineering, University of Alberta, Edmonton, Alberta, Canada T6G 2G6

Received: April 17, 2005; In Final Form: December 21, 2005

A theoretical model was developed on basis of nonequilibrium thermodynamics, dislocation kinetics, and electrochemistry, which may lead to the quantitative assessment of material loss produced by the synergism of mechanical and electrochemical factors in an erosion−corrosion process, As predicted by this model, the synergistic effect results mainly from the interaction of two irreversible fluxes, namely, the anodic dissolution current density and the plastic flowing in the surface layer caused by dynamic plastic deformation. An enhanced anodic dissolution flux is induced by the dynamic surface plastic deformation resulting from the impingement of solid particles, which can be correlated to the wastage rate due to the mechanical erosion. Meanwhile, the anodic current present at the electrode surface, in turn, can increase the mobility of dislocation and reduce the resistance in the surface layer against plastic deformation. Such an effect is demonstrated by the hardness degradation of metals in corrosive media. Theoretical analysis indicates that the corrosion-induced hardness degradation is a linear function of the logarithm of anodic current density. The degradation of mechanical erosion resistance with decreasing hardness suggests that the corrosion-enhanced erosion may result from the degradation in hardness of target material induced by the anodic dissolution and the corresponding wastage is also a linear function of the logarithm of anodic current density. The theoretical predictions were compared with the experimental results of carbon steels obtained form the slurry-erosion tests and the micro-hardness measurements. The results indicate that the hardness degradation in corrosive media is mainly controlled by the anodic current density and is almost independent of the polarization behavior of steels.

Introduction

In the slurry-erosion processes of metallic components, the material loss occurs, basically, through two different mechanisms. One results from the action of various mechanical forces on the surface, regarded as the erosion, and the material on the target surface is removed and enters the solutions before ionized, normally, in form of debris or chipping. Another is the result of electrochemical or chemical reactions, referred to as corrosion, and the metal is dissolved and leaves the surface in the form of ions or some other kind of corrosion product. In line with the mechanisms of material removal from the electrode surface, the rate of total material loss due to erosion−corrosion, $\dot{w}$, can be expressed as the sum of the contributions of the erosion component $\dot{e}$ and the corrosion component $\dot{c}$

$$\dot{w} = \dot{e} + \dot{c} \tag{1}$$

A large number of experimental investigations have indicated that the erosion resistance of materials in an inert environment mainly depends on their mechanical properties,[1] and the corrosion resistance is governed by their chemical characteristics.[2] In the slurry-erosion process, erosion and corrosion occur simultaneously. The damage mechanism is heavily dependent on the metallurgical features of a material[3−7] and the operating conditions including hydrodynamic parameters,[2,8] concentration and characteristics of erodents,[1,9−11] temperature, and corrosivity of the environment.[1,12] Several theoretical models were established for the mechanical erosion due to the impingement of solid particles[13−18] and for the electrochemical corrosion in fluid.[2,19−21] However, the complexity of the erosion−corrosion problem arises mainly from synergism owing to the interaction of mechanical and chemical factors.[22−24] In line with the mechanisms for material removal, the synergism can be further divided into the erosion-enhanced corrosion and the corrosion-enhanced erosion. Therefore, the wastages of erosion and corrosion in flowing slurries can be formulated as

$$\dot{e} = \dot{e}_0 + \dot{e}_c \tag{2}$$

$$\dot{c} = \dot{c}_0 + \dot{c}_e \tag{3}$$

where $\dot{e}_0$ is the erosion rate under corrosion-free conditions, $\dot{c}_0$ the corrosion rate when erosion is absent, $\dot{e}_c$ the component of corrosion-enhanced erosion, and $\dot{c}_e$ the component of erosion-enhanced corrosion. The synergism of erosion and corrosion, $\dot{w}_s$, is expressed as the sum of $\dot{e}_c$ and $\dot{c}_e$:

$$\dot{w}_s = \dot{e}_c + \dot{c}_e \tag{4}$$

Madsen[25] reported that 23−33% of the total weight loss of low-alloy steels could be attributed to the synergistic effect and that the contribution of synergism increased to 55−62% for 18−8 austenitic stainless steels. Yue et al.[26] found that, when the chrome white iron was eroded in low-pH slurry, the contribution of synergism could be as high as 86.3%. Although the synergism contributes to a substantial part of the total material loss in service, its mechanism is poorly understood due to the complexity of problem.[19,27]

When corrosion is controlled by the mass transportation of dissolved oxygen in a flowing solution, as summarized by

* To whom correspondence should be addressed. Telephone: (780) 492-2232. Fax: (780) 492-2881. E-mail: jingli.luo@ualberta.ca.

10.1021/jp051985f CCC: $33.50
Published on Web 02/10/2006

Poulson,[2,22] Heitz,[19] Postlethwaite,[28] and MacDonna et al.,[20] the corrosion rate in flowing slurries can be formulated with the hydrodynamic parameters of fluid and the diffusion coefficient of the oxidant. If there is a passive film/corrosion product scale on the surface, the corrosion rate will be affected by both mass transport processes in the surface film and the boundary layer of the fluid.[2,19,22] In this situation, the quantitative evaluation of the mass transport is still an unsolved problem.[19] Furthermore, depending on the opertating conditions and metallurgical features of materials, the mechanisms except for mass transportation, in many practical situations, may be the rate-determining step of the corrosion process. Recent research by the authors indicated that, in slurry-erosion of passive targets, the corrosion was likely to be controlled by the flux of particle impingement and kinetics of repassivation over the impacted area.[29] Sometimes, the corrosion mechanism transition will take place,[19,28] which makes the problem even more complicated.

There is still no quantitative model for the corrosion-enhanced erosion, although a few hypothesis have been proposed to explain this phenomenon qualitatively.[28,30−32] Neville et al.[23] and Bester et al.[30] pointed out that the preferential dissolution of a matrix in a flowing corrosive medium made the hard particles in the microstructure easy to be removed, resulting in acceleration of erosion. Besides the lack of quantitative description, this assumption is only suitable for the accelerated erosion in materials strengthened with hard phases but cannot explain the corrosion-enhanced erosion in single-phased materials, such as austenitic stainless steels. Some researchers[28,31,32] pointed out that an increase in surface roughness caused by corrosion would promote the synergistic effect. Experimental evidence[15,32,33] has shown that the wear resistance of metals degrades as the hardness and/or strength of materials is reduced. Matsumura et al.[32] suggested that the dissolution of a work-hardened layer on the target surface would degrade the erosion resistance of material. Although they did not give any quantitative relation between the erosion resistance and the corrosion kinetics, their point resembles the concept of the chemo-mechanical effect proposed by Gutman.[34] He pointed out that the resistance in the surface layer to the plastic deformation would be reduced when the material was being dissolved chemically or electrochemically.[34] According to the concept of chemo-mechanical effect, it is expected that the material will be less resistant to wear damage when corrosion is present. In light of this principle, a chemo-mechanical polish process has been developed for grinding hard materials.[35] Obviously, the chemo-mechanical effect may be a potential mechanism of corrosion-enhanced erosion. Unfortunately, this concept has not yet been explored in studies involving erosion corrosion.

Theoretically, failure process or property degradation of engineering materials is always related to certain irreversible thermodynamic processes. When erosion−corrosion occurs, at least two irreversible processes are involved: the electrochemical (or chemical) reactions at the electrode surface, which leads to corrosion, and plastic deformation in the surface layer caused by the impingement of solid particles, which results in erosion. These processes and their interaction can be assessed with the concepts of nonequilibrium thermodynamics. Based on the theory of nonequilibrium thermodynamics, Gutman[34] described the strength degradation of metals caused by the interaction of chemical and mechanical factors. Therefore, the primary aim of this paper is to study the synergistic mechanisms of the erosion−corrosion in active slurries, and an effort is made to model the interaction of mechanical and electrochemical factors in the slurry-erosion process with the aid of nonequilibrium thermodynamics, dislocation theory, and electrochemistry.

Theoretical Aspects for Synergism of Electrochemical and Mechanical Factors. *Some Basic Concepts of Non-Equilibrium Thermodynamics.* In accordance with the concepts of nonequilibrium thermodynamics,[36] all the factors resulting in the irreversible processes, such as stress, temperature gradient, concentration gradient, and electric potential gradient, are referred to as the generalized or thermodynamic forces F_i, (i = 1,2,...), and all the irreversible fluxes induced by the corresponding generalized forces, such as plastic flow, heat flow, diffusive flow, and electric current, are referred to as the generalized fluxes J_i (i = 1,2,...). It was known empirically that, for a large class of irreversible phenomena and under wide range of experimental conditions, the irreversible flows are linear functions of thermodynamic forces, such as Fick's first law for the diffusion caused by the concentration gradient and Fourier's law for the heat conduction induced by the temperature gradient. Also included in this kind of description are the linear laws for such cross-phenomena as the thermal diffusion and Dufour effect on the thermal conduction. Considering a system where m irreversible processes are involved, any irreversible phenomenon in this linear region is formulated with following phenomenological relationship:

$$J_i = \sum_{k=1}^{m} L_{ik} F_k, (i = 1,2,...,m) \tag{5}$$

where L_{ik} (i, k = 1,2,..., m) are the phenomenological coefficients. If the system is adiabatically insulated, its state can be described by a number of independent state variables, B_1, B_2,..., B_m. Under the equilibrium state, these parameters possess the values of B_1^0, B_2^0,..., B_m^0. The deviation of these state variables from their equilibrium values are given by

$$\beta_i = B_i - B_i^0 (i = 1, 2,..., m) \tag{6}$$

At the equilibrium, the entropy of the system has a maximum value and the deviation of the state variables β_1, β_2,..., β_m are zero by definition. In line with Onsager's theorem,[36] under a nonequilibrium state, the deviation of the entropy ΔS from its equilibrium value can be approximately given as

$$\Delta S = -\frac{1}{2} \sum_{i,k=1}^{m} g_{ik} \beta_i \beta_k \tag{7}$$

where g_{ik}(i,k = 1,2,..., m) are the second derivatives of ΔS with respective to the state variables β_i(i = 1,2,..., m) and they compose of a positive definite matrix. Under the nonequilibrium state, the entropy of the system tends to increase and the irreversible fluxes appear spontaneously. The generalized fluxes of irreversible processes, J_i, can be represented by the time derivatives of the state variables β_i,[36]

$$J_i = \dot{\beta}_i (i = 1,2,..., m) \tag{8}$$

and the thermodynamic forces corresponding to the fluxes, F_i, are given by the derivatives of entropy with respect to the state variables β_i

$$F_i = \frac{\partial S}{\partial \beta_i} = -\sum_{k=1}^{m} g_{ik} \beta_k (i = 1,2,..., m) \tag{9}$$

In line with eq 7, the time derivative of entropy, referred to as the entropy flow or strength of an entropy source, due to the irreversible processes occurring in the system, is formulated by

$$\dot{S} = -\sum_{i,k=1}^{m} g_{ik}\dot{\beta}_i\beta_k = \sum_{i=1}^{m} F_i J_i \tag{10}$$

So, the generalized forces and generalized fluxes can also be related to the entropy product in the following conjugated forms:

$$F_i = \frac{\partial \dot{S}}{\partial J_i}, (i = 1,2,..., m) \tag{11}$$

$$J_i = \frac{\partial \dot{S}}{\partial F_i}, (i = 1,2,..., m) \tag{12}$$

Consequently, the matrix of phenomenological coefficients must be symmetric,[36] i.e.,

$$L_{ik} = L_{ki}, (i,k = 1,2,..., m) \tag{13}$$

Equation 13 is referred to as the Onsager's reciprocity relations. If nonlinear processes, such as chemical reactions and plastic deformation, are involved, it is more convenient to use the affinities $A_i(1,2,..., m)$ and the entropy generation rate is expressed as follows:[34,36]

$$\dot{S} = \sum_{i=1}^{m} J_i \frac{A_i}{T} \tag{14}$$

T is the absolute temperature. In the case of $A_i \ll RT$ (R is the gas constant), the linear phenomenological equations are still approximately valid.[34]

$$J_i = \sum_{k=1}^{m} L_{ik} \frac{A_k}{T} \tag{15}$$

Irreversible Flux Induced by Plastic Deformation. It is well-known that plastic deformation of crystal results mainly from the irreversible dislocation movements. During the plastic deformation, the dislocations nucleate and move simultaneously. To simplify the analysis, the formation and movement of dislocation are considered as a unit process, i.e., once a dislocation nucleates, it moves immediately and then stops when encounters certain barriers. Assume λ to be the mean free path of dislocation movement and $\bar{V}$ the average velocity of dislocation movement. In accordance with the geometric analysis of plastic deformation, one can easily formulate the rate of plastic deformation $\dot{\gamma}_P$ as follows:[34,37]

$$\dot{\gamma}_P = \dot{N}b\lambda = Nb\bar{V} \tag{16}$$

where $\dot{N}$ is the dislocation nucleation rate, b is the Burgers vector, and N is the mobile dislocation density. Equation 16 indicates that the dislocation flux $\dot{N}$ can be regarded as the "reaction" flux of plastic deformation. Under the action of mechanical forces, dislocations can nucleate from various sites, such as the pinned dislocations (Frank−Read sources), grain boundaries, inclusions, and so on. In light of dislocation theory,[37,38] the probability for a Frank−Read (F−R) source being activated, p, can be expressed by following equation:

$$p = \nu \exp\left(-\frac{e_D - \tau v_D}{kT}\right) \tag{17}$$

where k is the Boltzmann's constant, ν is the vibration frequency of the dislocation segment, e_D is the height of the potential barrier to be overcome for activating the F−R source, τ is the applied shear stress, and v_D is the activation volume for a F−R source. A large number of test data[34,37] indicate that the dislocation density in crystals has a maximum value and the maximum possible dislocation density is about 10^{12}dislocations/cm^3. Denote N_{max} to be the maximum number of dislocations in a crystal with mass of one mole. By analogy with Avogadro's number N_A, N_{max} is regarded as 1 mole of dislocations, which has the dimension of "dislocations/mole of dislocations".[34] If the F−R sources are considered the only sites for dislocation nucleation, the nucleation rate of dislocations is formulated by

$$\dot{N} = N_{F-R}\nu \exp\left(-\frac{E_D - \tau V_D}{R_D T}\right) \tag{18}$$

where $E_D = N_{max}\, e_D$, $V_D = N_{max}\, v_D$, $R_D = kN_{max}$, N_{F-R} is the density of dislocation sources and τ is the shear flow stress which represents the strain hardening response of a metal to the dislocation movements. If the experimental conditions, including the test material, temperature, and environment, are held unchanged, an alternation of plastic deformation rate or in dislocation flux will result in a variation in the strain hardening response, and vice versa. In the dynamic plastic deformation process, a mobile dislocation must overcome the resistances resulting from the long-range stress field and short-range obstacles.[38,39] The former is often regarded as the internal stress τ_i, and it is due to the interaction of the dislocation with the long-range stress field produced by the other dislocations, grain boundaries, and precipitated particles. The latter comes mainly from the Peierls−Nabarro (P−N) stress τ_{P-N}, a resistance induced by short-range obstacles. Therefore, the flow stress τ can be considered the contributions of two components, one is athermal and another is thermal. For a first approximation, the flow stress can be expressed as the linear superposition of these two components,[40,41]

$$\tau = \tau_i(\gamma_P) + \tau_{P-N}(T, \dot{\gamma}_P) \tag{19}$$

The thermal fluctuation in a solid is not helpful for the mobile dislocation to overcome the resistance of long-range stress field, so that τ_i is an athermal variable and basically a function of plastic strain (γ_P) independent of the strain rate or dislocation flux. On the contrary, the active zone of the short-range stress has a size with the same order of magnitude as the atomic distance in lattice and the mobile dislocation can overcome the short-range obstacles with the aid of thermal fluctuation, so that, the τ_{P-N} is a function of temperature and dislocation flux (or plastic deformation rate). We define the "exchange" or "reversible" flux of dislocations $\dot{N}^0$ as

$$\dot{N}^0 = N_{F-R}\nu \exp\left(-\frac{W_D - \tau_i V_D}{R_D T}\right) \tag{20}$$

The irreversible flux of dislocations during the plastic deformation, $\dot{N}_P$, is given by definition as follows:

$$\dot{N}_P = \dot{N} - \dot{N}^0 = \dot{N}^0\left[\exp\left(\frac{\tau_{P-N} V_D}{R_D T}\right) - 1\right] \tag{21}$$

Obviously, $\dot{N}_P = 0$ when $\tau_{P-N} = 0$. By analogy with the approach to formulate the electrochemical reactions shown in next section, the affinity of plastic deformation A_P is defined as

$$A_P = \tau_{P-N} V_D \tag{22}$$

When $A_P = \tau_{P-N} V_D \ll R_D T$, we have the phenomenological coefficient for the plastic deformation

$$L_{11} = \frac{\dot{N}^0}{R_D} \tag{23}$$

where the subscript "1" represents the irreversible process caused by the plastic deformation. Thus, eq 21 can also be written as

$$\dot{N}_P = L_{11} R_D \left(\exp \frac{A_P}{R_D T} - 1 \right) = L_{11} R_D \left(\exp \frac{\tau_{P-N} V_D}{R_D T} - 1 \right) \tag{24}$$

The entropy generation rate due to plastic deformation is given by

$$\dot{S}_P = \dot{N}_P \frac{A_P}{T} \tag{25}$$

Irreversible Fluxes Caused by Corrosion Process. Consider a simple electrochemical process for anodic dissolution of a metallic electrode

$$\mathrm{Me} \leftrightarrow \mathrm{Me}^{z_M +} + z_M e^- \tag{26}$$

Its reaction flux is

$$J_M = J_M^0 \left[\exp\left(\frac{\alpha_M \tilde{A}_M}{RT} \right) - \exp\left(- \frac{(1-\alpha_M)\tilde{A}_M}{RT} \right) \right] \tag{27}$$

where α_M, J_M^0 and $\tilde{A}_M$ are the charge-transport coefficient, the exchange flux, and the electrochemical affinity for the oxidation reaction 26, respectively. J_M^0 can be regarded as the reversible fluxes of the anodic and cathodic half-reactions under the equilibrium condition. $\tilde{A}_M$ can be given by

$$\tilde{A}_M = \sum_i \nu_i \tilde{\mu}_i \tag{28}$$

In eq 28, ν_i is the stoichiometric coefficient and the electrochemical potential $\tilde{\mu}_i = \mu_i + zF\Delta\varphi$,where μ_i is the chemical potential, ($i = 1,2,....$), F is the Faraday's constant, $\Delta\varphi = \varphi - \varphi_0$, φ and φ_0 are the electrode potential and the equilibrium potential, respectively. The first and second terms on the left side of eq 27 are regarded as the fluxes of anodic and cathodic half-reactions, respectively. Under potential $\varphi \neq \varphi^0$, they can be expressed as the sum of reversible and irreversible fluxes. Therefore, the irreversible fluxes for the anodic and cathodic half-reactions of process 26 can be written respectively as[34]

$$J_{M,A} = J_M^0 \left[\exp\left(\frac{\alpha_M \tilde{A}_M}{RT} \right) - 1 \right] \tag{29}$$

$$J_{M,C} = - J_M^0 \left[\exp\left(\frac{(1-\alpha_M)\tilde{A}_M}{RT} \right) - 1 \right] \tag{30}$$

Let $\tilde{A}_M \ll RT$ and eqs 29 and 30 become

$$J_{M,A} = \frac{J_M^0 \alpha_M \tilde{A}_M}{R \quad T} \tag{31}$$

$$J_{M,C} = - \frac{J_M^0 (1-\alpha_M)\tilde{A}_M}{R \quad T} \tag{32}$$

$\alpha_M \tilde{A}_M$ and $(1 - \alpha_M)\tilde{A}_M$ can be regarded as the fractions of affinity for the anodic and cathodic half-reactions of process 26, respectively, In line with eq 15, the phenomenological coefficients for the reaction 26 are obtained as follows:

$$L_{22} = - L_{33} = \frac{J_M^0}{R} \tag{33}$$

where the subscripts "2" and "3" are used to represent the anodic and cathodic half-reactions of the process 26, respectively. As a result, eqs 29 and 30 are also rewritten as

$$J_{M,A} = L_{22} R \left[\exp\left(\frac{\alpha_M \tilde{A}_M}{RT} \right) - 1 \right] \tag{34}$$

$$J_{M,C} = L_{33} R \left[\exp\left(\frac{(1-\alpha_M)\tilde{A}_M}{RT} \right) - 1 \right] \tag{35}$$

Gutman[34] only considered the contribution of dissolution of metallic electrode to the entropy production of a corrosive system in his thermodynamic analysis for a corrosion reaction. Actually, during corrosion, the oxidation reaction of a metal, i.e., the process 26, always couples with a reduction reaction of certain oxidant in solution (O) which results in the formation of a reduction product (R):

$$O + z_O e^- \rightarrow R \tag{36}$$

Similarly, the irreversible fluxes of the anodic and cathodic half-reactions of process 36 can be expressed as

$$J_{O,A} = J_O^0 \left[\exp\left(- \frac{\alpha_O \tilde{A}_O}{RT} \right) - 1 \right] = L_{44} R \left[\exp\left(- \frac{\alpha_O \tilde{A}_O}{RT} \right) - 1 \right] \tag{37}$$

$$J_{O,C} = J_O^0 \left[\exp\left(- \frac{(1-\alpha_O)\tilde{A}_O}{RT} \right) - 1 \right] = L_{55} R \left[\exp\left(- \frac{(1-\alpha_O)\tilde{A}_O}{RT} \right) - 1 \right] \tag{38}$$

where α_O, J_O^0 and $\tilde{A}_O$ are the charge-transport coefficient, the exchange flux and the electrochemical affinity for the reduction reaction 36, respectively. The phenomenological coefficients L_{44} and L_{55} are given by

$$L_{44} = - L_{55} = - \frac{J_O^0}{R} \tag{39}$$

where the subscripts "4" and "5" stand for the anodic and cathodic reactions of process 36, respectively. The entropy flux induced by the electrochemical reactions involved in the corrosion process will be

$$\dot{S}_{EC} = J_{M,A} \frac{\alpha_M \tilde{A}_M}{T} + J_{M,C} \frac{(1-\alpha_M)\tilde{A}_M}{T} + J_{O,A} \frac{\alpha_O \tilde{A}_O}{T} + J_{O,C} \frac{(1-\alpha_O)\tilde{A}_O}{T} \tag{40}$$

In most corrosion systems of engineering practice, the self-corrosion potentials of systems are far away from the equilibrium potentials of metallic electrodes and the process 36, i.e., $J_{A,M} \gg J_{M,C}$ and $J_{O,A} \ll J_{O,C}$. The values of fluxes $J_{M,A}$ and $J_{O,A}$ are very small and their contributions to the entropy production are negligible. To simplify the analysis, the entropy flux is approximately written as

$$\dot{S}_{EC} \approx J_{M,A}\frac{\alpha_M \tilde{A}_M}{T} + J_{O,C}\frac{(1-\alpha_O)\tilde{A}_O}{T} \quad (41)$$

And the irreversible flux of anodic reaction $J_{M,A}$ can be approximately correlated to the anodic dissolution current density i_A using Faraday's secondary law:

$$i_A = z_M F J_{M,A} \quad (42)$$

where z_M is the number of moles of electrons released by the oxidation of one mole of metal, as indicated by anodic dissolution reaction 26.

Synergism of Mechanical and Electrochemical Factors. In the slurry-erosion process, the electrochemical corrosion of metallic electrode and the mechanical removal of surface layer (erosion) take place simultaneously. The surface layer of a metallic electrode must deform plastically before being removed by the impingement of solid particles.[13−16] The synergism of erosion−corrosion results from the interaction of the electrochemical dissolution and surface plastic deformation. Since both the electrochemical dissolution and plastic deformation are irreversible processes, they cause the entropy generation in the system and, if the open circuit potential for the system of interest is far way from the equilibrium potentials of processes (eqs 26 and 36), the total entropy generation is approximately formulated as

$$\dot{S} = \dot{S}_P + \dot{S}_{EC} = \dot{N}_P\frac{A_P}{T} + J_{M,A}\frac{\alpha_M \tilde{A}_M}{T} + J_{O,C}\frac{(1-\alpha_O)\tilde{A}_O}{T} \quad (43)$$

Under this condition, the effects of the cathodic half-reaction of process (eq 26) and the anodic half-reaction of process (eq 36) are approximately neglected and, in line with eq 5, the irreversible reaction fluxes will be approximately formulated by the following equations to take the cross effects of different processes into consideration:

$$\dot{N}_P = L_{11}R_D\left(\exp\frac{A_P}{R_D T} - 1\right) + L_{12}R\left(\exp\frac{\alpha_M \tilde{A}_M}{RT} - 1\right) + L_{15}R\left[\exp\left(-\frac{(1-\alpha_O)\tilde{A}_O}{RT}\right) - 1\right] \quad (44)$$

$$J_{M,A} = L_{21}R_D\left(\exp\frac{A_P}{R_D T} - 1\right) + L_{22}R\left(\exp\frac{\alpha_M \tilde{A}_M}{RT} - 1\right) + L_{25}R\left[\exp\left(-\frac{(1-\alpha_O)\tilde{A}_O}{RT}\right) - 1\right] \quad (45)$$

$$J_{O,C} = L_{51}R_D\left(\exp\frac{A_P}{R_D T} - 1\right) + L_{52}R\left(\exp\frac{\alpha_M \tilde{A}_M}{RT} - 1\right) + L_{55}R\left[\exp\left(-\frac{(1-\alpha_O)\tilde{A}_O}{RT}\right) - 1\right] \quad (46)$$

The reduction half-reaction of process (eq 36), in an anodic dissolution system, only relates to the affinity of ions in solution and it is not affected by the plastic deformation of solid electrode. Therefore, $L_{15} = L_{51} = 0$ and eq 44 is simplified as follows:

$$\dot{N}_P = L_{11}R_D\left(\exp\frac{A_P}{R_D T} - 1\right) + L_{12}R\left(\exp\frac{\alpha_M \tilde{A}_M}{RT} - 1\right) \quad (47)$$

The second term in eq 47 expresses the influence of anodic dissolution on the mobility of dislocations. Since the reactions in eqs 26 and 36 are independent, electrode processes and no synergistic effect exists, $L_{25} = L_{52} = 0$. In this situation, eq 46 will be the same as eq 38 and eq 45 becomes

$$J_{M,A} = L_{21}R_D T\left(\exp\frac{A_P}{R_D T} - 1\right) + L_{22}RT\left(\exp\frac{\alpha_M \tilde{A}_M}{RT} - 1\right) \quad (48)$$

The first term in eq 48 represents the increment in anodic dissolution rate induced by the plastic flow of the solid electrode, denoted as ΔJ_A, and the second term of eq 48 is the irreversible dissolution flux on the electrode surface free of plastic deformation. Duquette[42] reported that both the intensity and localization of surface plastic deformation were enhanced by anodic dissolution and the slip bands were more likely to be attacked. This observation indicates that there is the interaction of plastic deformation and anodic dissolution and the interaction intensity for the mechanical and electrochemical factors $L_{12} = L_{21} \neq 0$. Actually, many experimental investigations have indicated that the corrosion of metallic electrodes will be accelerated while the plastic deformation was going on.[34,43,44] This phenomenon of dynamically plastic deformation-promoted corrosion is referred to as the mechano−chemical effect[34] and its contribution to the anodic dissolution is given as

$$\Delta J_A = L_{21}R_D T\left(\exp\frac{A_P}{R_D T} - 1\right) \quad (49)$$

Substituting eqs 16 and 23 into eq 49, we have

$$\Delta J_A = \frac{L_{21}}{L_{11}}\dot{N}_P = \frac{L_{21}}{L_{11}b\lambda}\dot{\gamma}_P \quad (50)$$

Equation 50 suggests that the anodic dissolution current density increases linearly with the plastic deformation rate. This was experimentally confirmed by Gutman[34] and Bockris et al.[45] Because of the mechano−chemical effect, it is expected that the corrosion process during slurry erosion should be promoted by the impingement of solid particles, as previously confirmed by experimental observations.[9,10,11]

Since $L_{12} \neq 0$, eq 47 indicates that the anodic dissolution present on the surface will induce an extra dislocation flux in the surface layer. It suggests the existence of chemo−mechanical effect. The corrosion-promoted plasticity due to the chemo−mechanical effect has been found in austenitic steel,[46,47] copper,[48] magnisium alloy,[49] cadium,[34] and brass.[50] The reasearchers found that the creep rate of samples at room temperature increased as anodic current was applied,[34,46,48,50] and it would recovered its original value after the current was shut-off.[34,48] Gutman,[34] Revie and Uhlig[48] believed that the anodic generation of a supersaturation of subsurface vacancies was responsible for this phenomenon. Theoretical analysis and experimental evidence have indicated that supersaturation vacancies may be produced by selective dissolution of the surface and it can promot diffusion in the surface layer.[46,51,52] The generation of vacancies could attenuate the strain-hardening in subsurface and enhance the localized surface plasticity.[46] The injection of vacancies from surface due to the anodic dissolution is likely to bring about a chemical potential gradient for the dislocations in the surface layer.[50] The chemical potential gradient may result in an additional dislocation flux in this layer.[34] This has been confirmed by the experimental observations.[34,42,53] Due to the fact that the mean free path of dislocation possesses a limited value, only the dislocation situated in the surface layer with a depth less than or equal to the mean free path can reach the surface, so that the chemo−mechanical effect can affect mainly the mechanical properties in this surface layer. This point has

been demonstrated by the fact that the anodic dissolution-enhanced creep is more readily observed in stressed thin wires or foils.[34,47,48]

Mechanical Property Degradation in Surface Layer Caused by Anodic Dissolution. Let's consider a dynamic deformation process of a sample with a stable deformation rate under the action of applied stress. Assume that the dislocation flux within the surface layer is $\dot{N}_P^*$ and the corresponding response of Peierls−Nabarro stress is $\tau_{\mathrm{P-N}}^*$ while the anodic current is absent. Once an anodic current i_A is applied to create an irreversible flux of anodic dissolution, the anodic dissolution-induced dislocation flux $\dot{N}_A$ appears in the surface layer owing to the chemo−mechanical effect. If the overall plastic flow rate or the total dislocation flux is kept unchanged by adjusting the applied stress, the dislocation flux produced by the mechanical force will change from $\dot{N}_P^*$ to $\dot{N}_P^{**}$ and the response of Peierls−Nabarro stress will become $\tau_{\mathrm{P-N}}^{**}$. Obviously, in this situation

$$\dot{N}_P^* = \dot{N}_P^{**} + \dot{N}_A \tag{51}$$

Because the Peierls−Nabarro stress $\tau_{\mathrm{P-N}}$ decreases as the dislocation flux induced by the mechanical force is reduced, the attenuation of strain hardening (or flow stress) due to the anodic dissolution $\Delta\tau_A$ is given as

$$\Delta\tau_A = \tau_{\mathrm{P-N}}^{**} - \tau_{\mathrm{P-N}}^* < 0 \tag{52}$$

The dislocation fluxes before and after applying the anodic current can be formulated with eqs 24 and 47. Insert eqs 24 and 47 into eq 51 and we have

$$L_{11}R_D\left(\exp\frac{\tau_{\mathrm{P-N}}^* V_D}{R_D T} - 1\right) = L_{11}R_D\left(\exp\frac{\tau_{\mathrm{P-N}}^{**} V_D}{R_D T} - 1\right) + L_{12}R\left(\exp\frac{\alpha_M \tilde{A}_M}{RT} - 1\right) \tag{53}$$

Adjust the anodic dissolution rate to eliminate the strain hardening effect ($\dot{N}_P^{**} = 0$), i.e., to make the dislocation flux induced by applying anodic current dissolution to compensate fully that produced solely by the mechanical force, eq 53 will become

$$L_{11}R_D\left(\exp\frac{\tau_{\mathrm{P-N}}^* V_D}{R_D T} - 1\right) = L_{12}R\left(\exp\frac{\alpha_M \tilde{A}_M}{RT} - 1\right) = \frac{L_{12}}{L_{22}}J_{M,A} \tag{54}$$

In this case, $\tau_{\mathrm{P-N}}^{**} = 0$, $\Delta\tau_A = -\tau_{\mathrm{P-N}}^*$. Note that eq 34 is used in the transition at the right side of eq 54. To display the dependence of degradation on the anodic dissolution rate, eq 54 is reorganized as follows

$$\Delta\tau_A = -\frac{R_D T}{V_D}\ln\left(1 + \frac{J_{M,A}}{J_{th}}\right) = \frac{kT}{\upsilon_D}\ln\left(1 + \frac{J_{M,A}}{J_{th}}\right) \tag{55}$$

J_{th} is a threshold irreversible flux of the anodic dissolution to induce the chemo−mechanical effect

$$J_{th} = \frac{L_{22}L_{11}R_D}{L_{12}} = \frac{J_M^0 \dot{N}^0}{L_{12}R} \tag{56}$$

Under the state far away from the equilibrium potential, which is common to most erosion−corrosion processes, $J_{\mathrm{M,A}}$ is several orders greater than J_{th}, so that eq 55 can be approximately simplified into the following form if eq 42 is applied

$$\Delta\tau_A \approx -\frac{R_D T}{V_D}\ln\left(\frac{J_{M,A}}{J_{th}}\right) \approx -\frac{kT}{\upsilon_D}\ln\left(\frac{i_A}{i_{th}}\right) \tag{57}$$

where $i_{th} = z_M F J_{th}$. Equation 57 indicates that the strength degradation of the surface layer due to the chemo−mechanical effect is approximately a linear function of the logarithm of anodic current density on the surface.

Because the anodic dissolution-induced surface strength is difficult to measure directly with experimental methods, it is important to find an equivalent parameter to evaluate the chemo−mechanical effect. Many experimental results have indicated that the yield strength of steels can be correlated to their hardness.[54] During the loading process of hardness measurements with a conical or pyramidal indenter, a quadratic relation is usually found between the load P and penetration depth h:[55,56]

$$P = Kh^2 \tag{58}$$

where the parameter K is dependent on the geometry of indenter and mechanical properties of the test material. For the Vickers hardness measurement, the standard tetrahedral pyramid indenter is adopted. Once the real area of impression A left by the maximum indenting load $P_{\max}$ is known, the Vickers hardness can be calculated as follows:

$$H\upsilon = \frac{P_{\max}}{A} = \frac{2P_{\max}}{\bar{d}^2}\sin\left(\frac{\theta}{2}\right) \tag{59}$$

$\bar{d}$ is the average diagonal length of projected area of impression. The θ value of Vicker's hardness indenter is 136°. In line with the impression geometry, the impression depth $h_c = d\tan(\theta/2)/\sqrt{2}$, so that eq 59 becomes

$$H\upsilon = K\sin\left(\frac{\theta}{2}\right)\cos^2\left(\frac{\theta}{2}\right) \tag{60}$$

The K value depends on the mechanical properties of material. According to the experimental results summarized by Sakai et al.,[56] $K \propto \sigma_{ys}$. So

$$H\upsilon = Y\sigma_{ys} = Y\upsilon\tau_{ys} \tag{61}$$

where Y is a material constant σ_{ys} and τ_{ys} are the tensile and shear yield strength, υ is the orientation factor. For an isotropic material under the uniaxial tensile condition, $\upsilon = 0.5$.[57] Normally, it is believed that the metal is incompressible and its plastically flowing behavior obeys von Mises criterion. In this situation $Y\upsilon = \sqrt{3}$.[58] Inserting eq 61 into eq 57, we have

$$\Delta H_\upsilon = H\upsilon_c - H\upsilon = -\frac{Y\upsilon kT}{\upsilon_D}\ln\left[\frac{i_A}{i_{th}}\right] \tag{62}$$

where $H\upsilon$ and $H\upsilon_c$ are the hardness values measured in air and corrosive environment. In line with above analysis, $H\upsilon_c < H\upsilon$ and $\Delta H\upsilon < 0$. The activation volume of the dislocation source is the key parameter to evaluate the anodic dissolution-induced hardness degradation. Unfortunately, at this moment it is still difficult to accurately calculate the value of υ_{D}, although it is sometimes assumed to be proportional to the mean free path of precipitates in steels. Since the activation volume of dislocation source is a parameter depending only on the nature of target

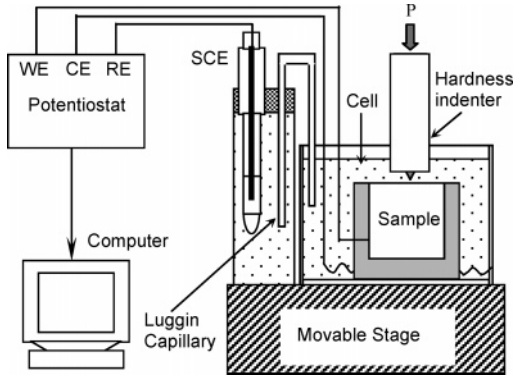

Figure 1. Schematic illustration of measurement system to measure micro-hardness with the presence of anodic current.

material, the anodic dissolution-induced hardness degradation is expected to be a linear function of logarithm of anodic current density.

Experimental Section

Hardness Measurements Under Anodic Polarization Conditions. Five carbon steels, namely, X52, X70, X100, A1018, and A1045, were used in the hardness measurement. To determine the dependence of hardness on the anodic current density, the test setup shown in Figure 1 was adopted. A conventional three-electrode cell, where a platinum wire was used as the counter electrode and a saturated calomel electrode (SCE) as the reference electrode, was fixed on the movable stage of hardness tester. The applied anodic polarization currents were controlled by an EG&G potentiostat. Prior to the hardness measurements, the epoxy mounted sample was polished mechanically, rinsed with deionized water and acetone, and then fixed in the cell containing the test solution. The Vickers microhardness of steel samples was measured with a Shimazhu microhardness tester under the action of indenting load of 200 g while anodic current was applied under galvanostatic control. The time for applying indenting load was 15 s. To reduce the effect of roughness induced by corrosion on the measurement of the indent area, only one hardness datum was measured on each specimen, and the hardness measurements under each condition were repeated on five different specimens. The indenting load was applied immediately after the anodic current was turned on and, as soon as the loading process was completed, the applied current was turned off. The test solution was drained from the electrochemical cell and the sample surface was dried with a paper wiper before measuring the diagonal length of projected area of impression. Test solutions were deionized water and aqueous solution of 1 M $NaHCO_3$. The polarization behavior of test materials was active in the deionized water but displayed an active-to-passive transition behavior in aqueous solution of 1M $NaHCO_3$.

Erosion-Corrosion Test. Test material used in erosion−corrosion tests was A1018 carbon steel. To achieve different hardness in samples for the erosion tests, a set of samples were annealed at different temperatures in flowing nitrogen for 1 h. The microstructures of the steel under both as-received and annealed conditions were typical ferrite + pearlite microstructure. The erosion−corrosion tests were conducted in the slurries comprising silica sand and process recycle-cooling water used in oil sand production, which was offered by Syncrude Ltd, Canada. The chemical composition of the process recycle-cooling water is given in Table 1. The sand concentrations of

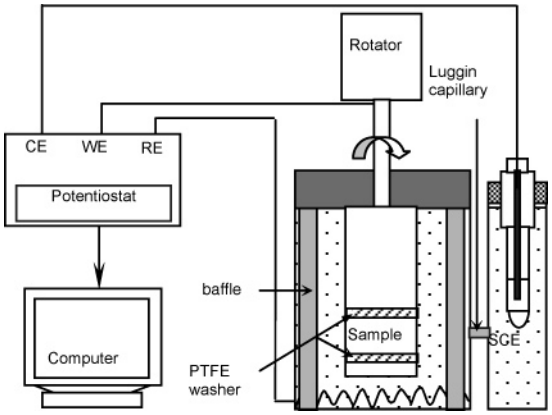

Figure 2. Schematic illustration of the erosion-corrosion test setup.

TABLE 1: Chemical Composition of the Process Recycle-Cooling Water (pH=8.05)

cation	Na^+	K^+	Ca^{2+}	Mg^{2+}
mg/L	727	11.3	6.8	4.0
Anion	Cl^-	SO_4^{2-}	HCO_3^-	CO_3^{2-}
mg/L	380	211	950	<5

slurries were in the range of 6.5 to 60 wt % The sand was commercially available ungrounded silica sand (U. S. Silica Company, Ottawa). Its size was 50−70 mesh (300−212μm).

The custom-made rotating cylinder electrode (RCE) system was used in erosion−corrosion tests, as indicated in Figure 2. Four baffles were mounted 90° to each other on the side the cell to minimize vortex formation and axial flow in the slurry. Polytetrafluoroethylene (PTFE) washers were used to prevent crevice corrosion of specimens. The rotating speeds of the RCE adopted were in a range from 2000 to 12 000 rpm. The apparent flow rate is $U = \dot{\omega}r$, where $\dot{\omega}$ is the rotating angle speed and r is the radius of the specimen. The thickness and outer diameter of the cylinder samples were 8 mm and 25 mm, respectively. A platinum counter electrode ring was placed near the bottom of the corrosion cell to cease its perturbation on the flow field. SCE was used as the reference electrode which was connected to the cell with a luggin capillary. The self-corrosion current densities were determined from the polarization curves under the test conditions which were measured with a potential scanning rate of 1 mV/s.

The pure erosion tests were measured under the potential of −0.9 V vs SCE to guarantee full cathodic protection. The erosion−corrosion tests were divided into two groups, one group was carried out under the open circuit potential and another one was conducted under the galvanostatic conditions with the applied current densities in the range 1×10^{-5}A/cm^2 to 5×10^{-4}A/cm^2. The latter test group was designed to measure the wastage rate of corrosion-enhanced erosion. When the applied potentials are several tens of millivolts, the uniform electrochemical corrosion rate during the galvanostatic tests was fully under the control of the applied anodic currents. In this situation, the wastage rate due to electrochemical corrosion can be determined from the applied anodic current densities using Faraday's secondary law

$$\dot{c} = J_{M,A} = \frac{i_A}{z_M F} M \tag{63}$$

where M is the atomic weight of metallic electrode on which the anodic dissolution reaction (eq 26) takes place. Because the corrosion rate under galvanostatic condition was not affected by the mechanical erosion, the total weight loss rate $\dot{w}$ under

the galvanostatic condition should be the sum of contributions of pure erosion, corrosion, and corrosion-enhanced erosion. The corrosion-enhanced erosion could be estimated by following equation

$$\dot{e}_c = \dot{w} - \dot{e}_0 - \dot{c} \tag{64}$$

At the open circuit potential, the corrosion rates were calculated, using the Faraday's secondary law, from the self-corrosion current densities, i_{corr}. In line with eq 3, the wastage component of erosion-enhanced corrosion was calculated as follows:

$$\dot{c}_e = \dot{c} - \dot{c}_0 = \frac{M}{z_M F}(i_{corr} - i_{corr,0}) \tag{65}$$

where $i_{corr,0}$ is the self-corrosion current density of the metallic electrode in flowing electrolyte without solid particles.

Before measuring the initial mass of a sample, the surface was ground, washed, and dried. After the initial mass measurement, a lacquer coating was used to protect the top and bottom surfaces of cylindrical specimens from crevice corrosion. After the erosion-corrosion test completed, the corrosion product on the specimen surface was cleaned according to the ASTM Standard G1−90. Aqueous solution of hydrochloric acid + hexamethylene tetramine (inhibitor) was used to remove the corrosion product on the test surface. Then, the lacquer coating on the specimens was dissolved with acetone. Before measuring the final mass, the samples were rinsed by deionized water and acetone, successively, and then dried in flowing air. The masses of samples were measured with a precision analytical scale with accuracy of 0.1 mg.

Results

Anodic Dissolution-Induced Hardness Degradation. The dependences of hardness of five carbon steels on anodic current density are demonstrated in Figure 3, where the anodic dissolution-induced hardness degradation ΔHv has been normalized with the original hardness Hv. The results show clearly that the hardness of steels decreases with an increase in the anodic current density and, as predicted by eq 62, the hardness degradation is a linear function of the logarithm of the anodic current density, since the activation volume of dislocation source is regarded as a material constant. Moreover, Figure 3 also indicates that the dependence of the hardness on the anodic current density measured in the two test solutions is quite similar, although the test materials display different polarization behavior. This simply implies that the chemo−mechanical effect depends mainly on the anodic current density but is essentially independent of the polarization behavior of the test materials.

Erosion, Corrosion and Synergism in Slurry-Erosion. Figure 4 shows that the total material loss rate, as well as the wastage caused by mechanical erosion and electrochemical corrosion, at the open circuit potential, increases with the flowing rate and sand concentration of slurries, C_s. The percentage contributed by each component to the total material loss of erosion−corrosion is depicted in Figure 5. The contribution of the pure mechanical erosion increases but that of corrosion-enhanced erosion decrease monotonically with the increases of flow rate and sand concentration. In the present study, the wastage of pure corrosion was defined as the material loss in flowing corrosive medium without solid particles. Therefore, when the flowing rate was kept constant, the component of pure corrosion is unchanged. The relative contribution of each component depends on the hydrodynamic conditions. Under the test conditions of the present study, the total wastage due to the electrochemical corrosion only occupies less than 1% of total material loss. This fact indicates that the erosion mechanism dominates the erosion−corrosion processes under the current test conditions. Figure 5 also indicates that, although the wastage produced by corrosion is only a small part of total material loss, it can accelerate the erosion process significantly. The relative contribution of corrosion-enhanced erosion in the total material less is more pronounced in the slurries with low sand concentration and with relatively low flowing velocity. It suggests that, when the slurry pipes of carbon steel are eroded in near-neutral pH slurries, as often happens in engineering practice, the electrochemical corrosion significantly accelerates the erosion process. Therefore, the mechanism of chemo−mechanical effects should be well understood to accurately assess the service life of the pipes.

The results in Figure 4 show that the pure mechanical erosion is mainly controlled by mechanical factors, such as increasing impact frequency of solid particles due to high sand concentration and increasing momentum of solid particles resulting from the high flowing velocity. When the sand concentration is held constant, as indicated by Figure 6, the dependence of pure erosion rate on the apparent flow rate of slurry U can be approximately expressed in following form

$$\dot{e}_0 = \kappa_U U^{n_U} \tag{66}$$

where κ_U and n_U are experimental constants.

As the hardness of the steel is reduced, the material loss rate due to mechanical erosion increases owing to a decrease in the resistance of materials to the plastic deformation, as shown in Figure 7. This agrees with the experimental results summarized by Hutchings,[15] Madsen,[25] and Heitz.[19] Some researchers[27] did not find the correlation between the hardness and the erosion−corrosion resistance. The reason for this may be related to the test conditions. If the erosion tests are not conducted under the fully cathodic-protected conditions, the contribution of corrosion-related components on the total material loss will be observed. If the corrosion-related mechanisms dominate the erosion−corrosion processes, it will be unlikely to find the dependence of total material loss on the hardness of material. On the other hand, some researchers[15,27] attempted to find the relationship between the erosion resistance and hardness in different kinds of materials or materials with broad variations in both chemical composition and microstructure. A large number of experimental researchers, however, have indicated that the composition and microstructure often display a significant influence on the wear mechanism, resulting in a big difference in the dependence of wear-resistance on the mechanical properties of materials.[59,60]

Under the hydrodynamic conditions for the current experiments, the dependence of the material loss rate due to mechanical erosion ($\dot{e}_0$) on the hardness shown in Figure 8 can be approximately formulated as follows

$$\dot{e}_0 = \kappa_H Hv^{-n_H} \tag{67}$$

where κ_H and n_H (>0) are the constants determined by experiments. According to eqs 66 and 67, the mechanical erosion rate can be formulated by following empirical expression

$$\dot{e}_0 = \kappa U^{n_U} Hv^{-n_H} \tag{68}$$

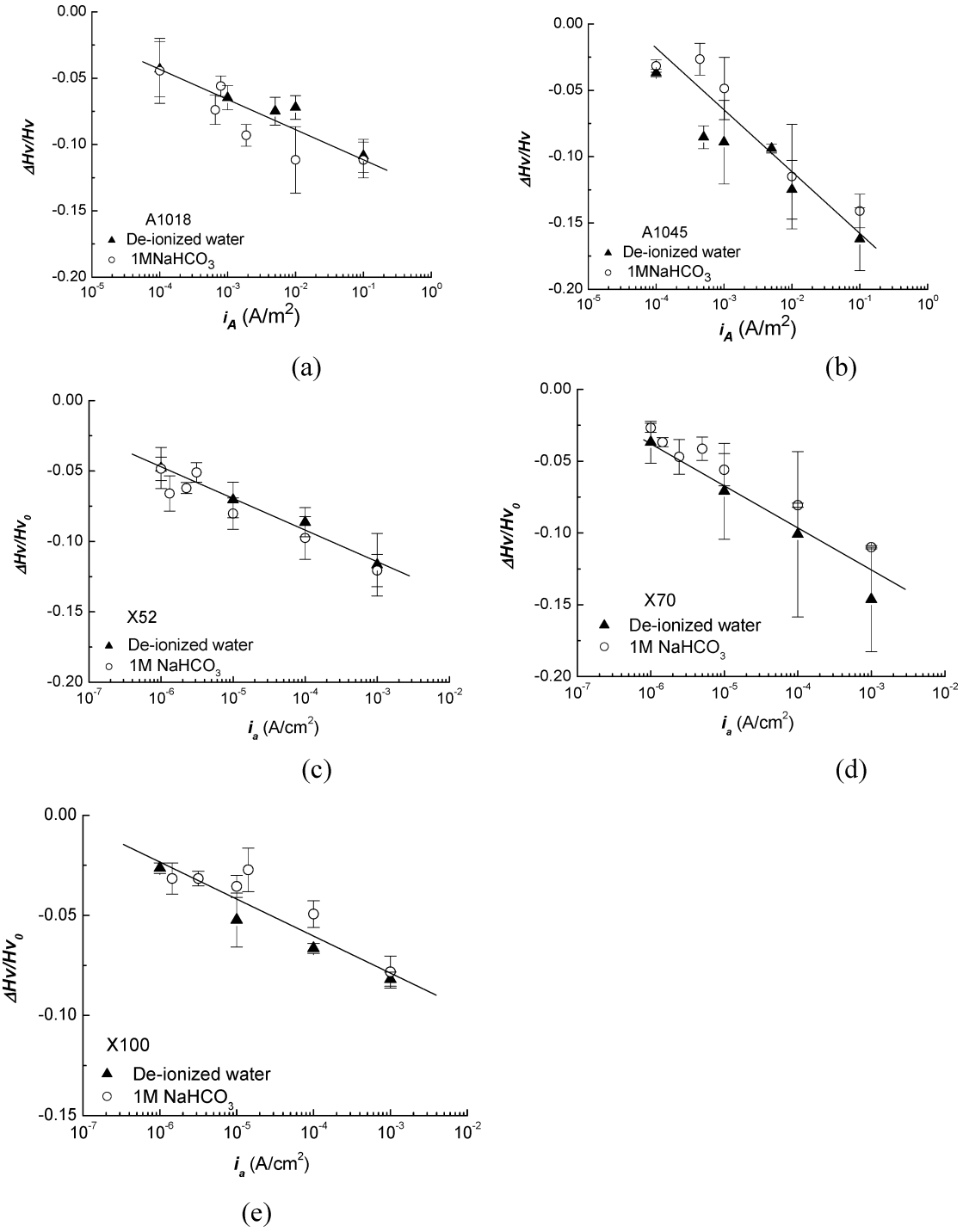

Figure 3. Relationship between the normalized hardness drop and anodic current density.

κ is an experimental constant. Figure 7 indicates $n_U \approx n_H$, so that eq 68 is rewritten as

$$\dot{e}_0 = \kappa\left(\frac{U}{Hv}\right)^n \tag{69}$$

n is also an experimental constant. As shown in Figure 8, the value of $\dot{e}_0$ increases monotonically with the ratio of U/Hv. Theoretically, the erosion wastage increases linearly with the solid concentration at a constant flowing velocity in dilute slurries if the solid particles are uniformly distributed. Because the solid particles in a slurry of the rotating cylinder system are not uniformly distributed, the actual sand concentration on the specimen surface differs from the nominal one, so that no attempt was made to correlate the erosion wastage to the nominal sand concentration.

Application of Theoretical Model to Evaluate the Synergism in Erosion-Corrosion. *Corrosion-Enhanced Erosion.* It has been well recognized that the corrosion will be promoted when the flow rate of corrosive media and the sand concentration in slurries are increased.[2,9,10,11,19,20,22,28] According to the concept of the chemo−mechanical effect, the surface layer of metals exposed to corrosive medium will soften and it will result in the degradation of erosion resistance. If the increasing erosion rate caused by the anodic dissolution-induced hardness degradation is the only mechanism of corrosion-enhanced erosion, the increment of erosion rate $\Delta\dot{e}$ due to the presence of anodic

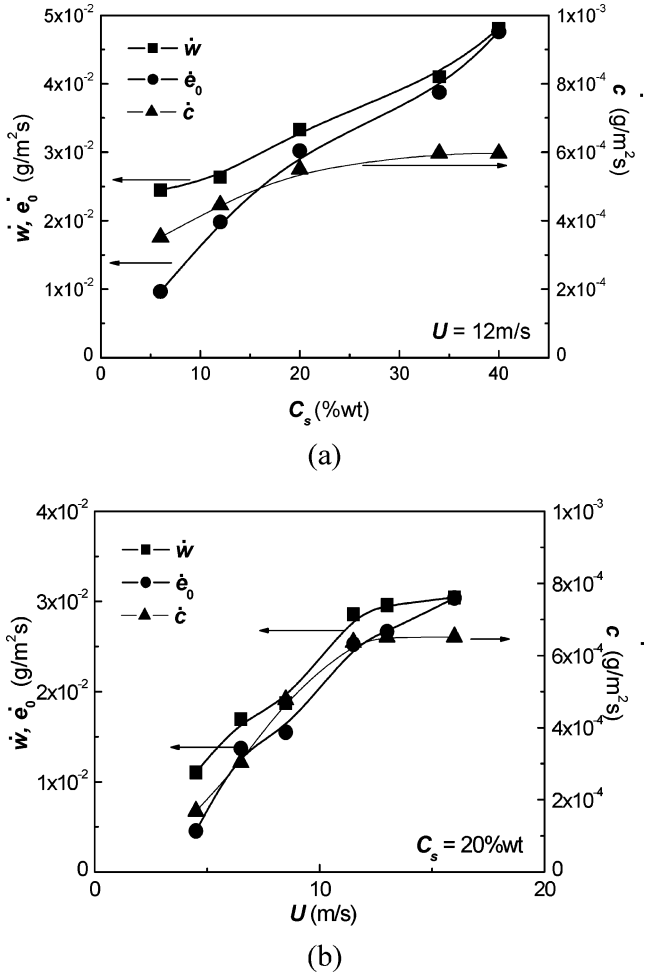

Figure 4. Effect of flowing velocity and sand concentration on erosion−corrosion behavior.

dissolution is defined as the corrosion-enhanced erosion, i.e., $\dot{e}_c = \Delta\dot{e}_0 = \dot{e} - \dot{e}_0$. If the test condition (including flow condition, sand concentration, and temperature) is held unchanged, in line with eq 69, we have

$$\dot{e}_c = \Delta\dot{e}_0 = \kappa U^n (Hv_c^{-n} - Hv^{-n}) = \dot{e}_0\left[\left(\frac{Hv_c}{Hv}\right)^{-n} - 1\right] \approx -n\dot{e}_0\left(\frac{\Delta Hv}{Hv}\right) \quad (70)$$

In the approximation at right end of eq 70, the first Taylor polynomial was adopted. Substitute eq 62 into eq 70 and reorganize it, then

$$\frac{\dot{e}_c}{\dot{e}_0} = \frac{nkT}{\upsilon_D Hv}\left(\frac{i_A}{i_{th}}\right) \quad (71)$$

According to eq 71, the erosion will be enhanced by the chemo−mechanical effect when corrosion occurs simultaneously and the normalized corrosion-enhanced erosion rate $\dot{e}_c/\dot{e}_0$ will increase with increasing anodic dissolution rate and the relationship between them can be approximately formulated as a linear function of the logarithm of anodic current density. It is confirmed by the experimental data in Figure 9.

However, the values of $\dot{e}_c$ estimated with eq 71 are lower than those experimentally determined, as shown in Figure 10 for instance. The authors believed that at least three reasons could be attributed to this deviation.

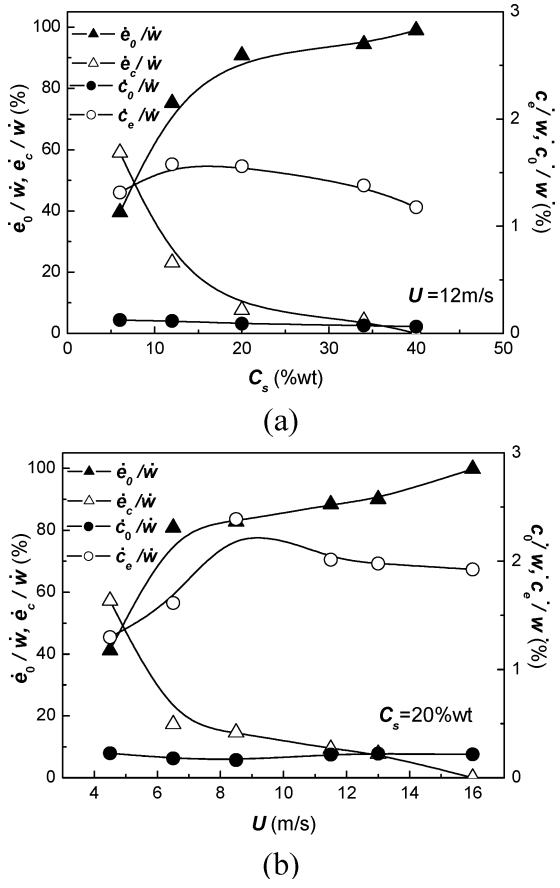

Figure 5. Relative contributions of wastage components to total material loss.

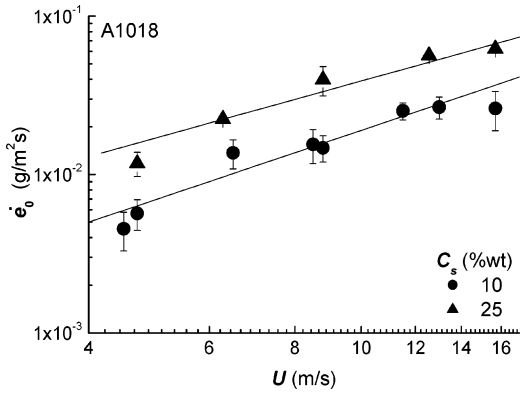

Figure 6. Dependence of mechanical erosion rate on the apparent flow velocity of slurries.

The first possible reason may relate to the synergistic mechanisms other than the anodic dissolution-induced erosion resistance degradation operating in slurry-erosion processes. In this case, $\dot{e}_c > \Delta\dot{e}_0$, so eq 70 will underestimate the material loss caused by the chemo−mechanical effect. Recent experimental investigations in the author's laboratory[61] indicated that, in flowing corrosive media free of solid particles, the material loss measured with the traditional weight loss method ($\dot{w}_{exp}$) was always higher than that calculated with Faraday's second law ($\dot{w}_{pred}$) but both agreed very well if the tests were conducted in quiescent solutions. The difference in the material loss rate $\Delta\dot{w}(= \dot{w}_{exp} - \dot{w}_{pred.})$ was regarded as the non-Faraday wastage, because it could not be predicted by Faraday's secondary law. When the corrosion in the flowing corrosive media was suppressed by the cathodic protection, the weight loss of specimens was almost undetectable. This implied that the non-

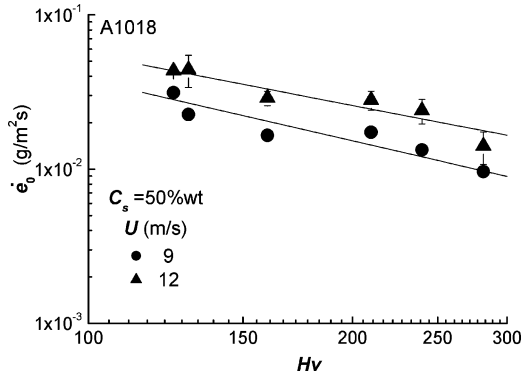

Figure 7. Dependence of mechanical erosion rate on hardness of steels.

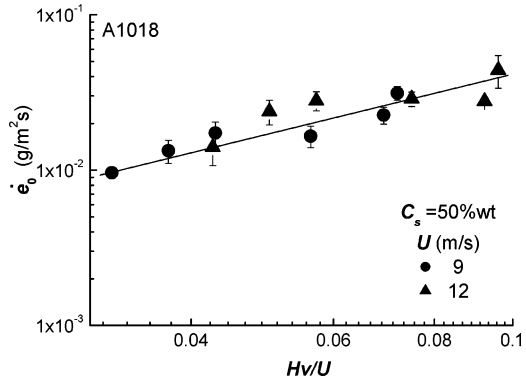

Figure 8. Relationship between mechanical erosion rate and U/Hv.

Faraday wastage was unlikely to result from cavitation erosion, because the cavitation erosion could not be suppressed by the cathodic protection. The non-Faraday wastage increased with the flow velocity and varies linearly with the logarithm of applied anodic current density, suggesting it is also caused by the interaction of mechanical and electrochemical factors. However, this non-Faraday wastage could not be formulated with eq 70 because the corrosion-enhanced erosion cannot be observed when erosion is absent. The experimental results indicated that this non-Faraday wastage is always less than the Faraday one. The data in Figure 4 show that the corrosion wastage is only a few percent of the total material loss, so the contribution of non-Faraday wastage should be very limited.

The second possible reason may be that the load used in the hardness measurement was too high so that the depth of indentation was much greater than those of wear scratches produced by sand particle impingement. It has been mentioned in the previous section that the anodic current on the surface can only affect the mechanical properties of the very thin layer on the specimen surface, i.e., within thickness less than the mean free path of dislocations. Therefore, the hardness degradation in the surface layer of electrode was underestimated when the experimental data in Figure 3 were used, obtained with the micro-hardness technique, to characterize the effect of anodic dissolution on the erosion resistance of material. To guarantee that the indent depth is smaller than the mean free path of mobile dislocations in the surface layer, the nano-indentation technique has been used to determine the real response of dislocation mobility in the surface layer to the chemo−mechanical effect. The result (not show here) has indicated the hardness degradation caused by the anodic dissolution is reduced with increasing indent load used in the hardness measurement and the relative hardness degradation due to anodic dissolution $\Delta Hv/Hv$ can reach 50%, which is 2−3 times as high as that measured with the micro-hardness technique.

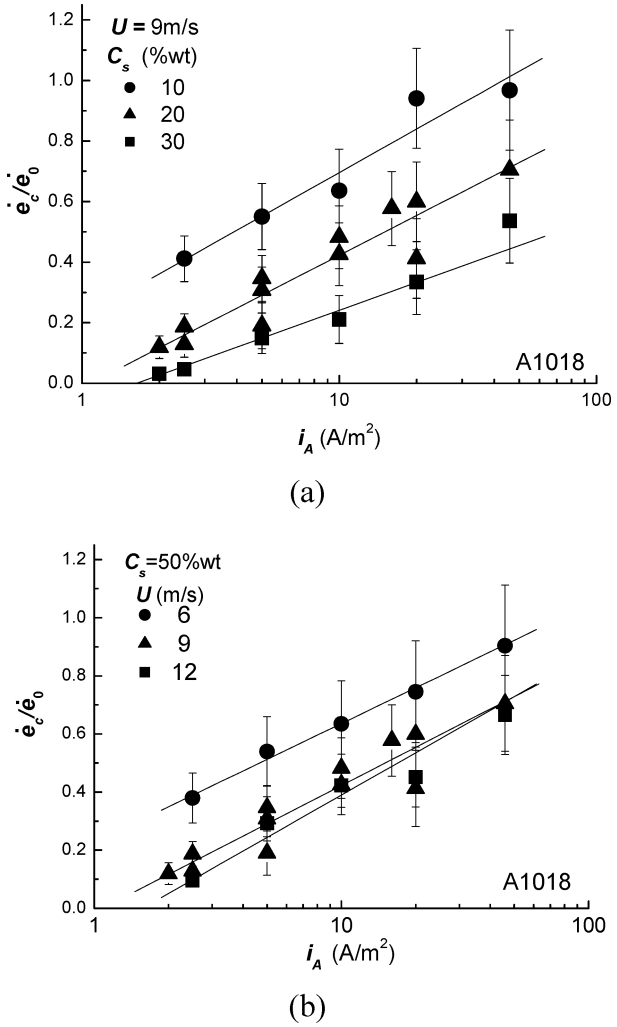

Figure 9. Effect of anodic current density on normalized corrosion-enhanced erosion rate.

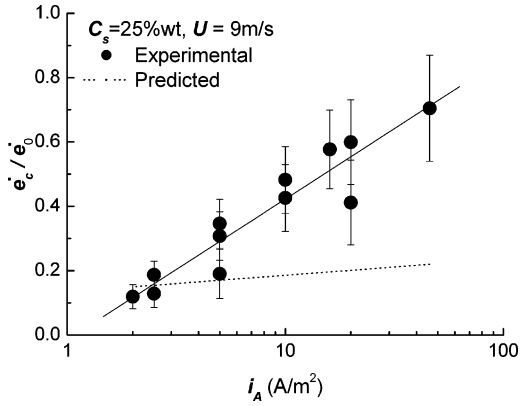

Figure 10. Comparison between the experimentally measured and predicted values of $\dot{e}_c/\dot{e}_0$.

The other possible reason may be attributed to the nonuniform distribution of anodic dissolution rate in microscale. The electrochemical noise detected during slurry-erosion process is shown in Figure 11. The transient current peaks resulted from the impingement events of sand particles and the peak value of local anodic current density $i^L_{A,peak}$ over the fresh surface of wear scars during scratching by the impingement of sand particles was much higher than the average current density on the whole electrode surface i_A.[62−64] The corrosion-enhanced erosion occurs while sand particles are scratching the electrode

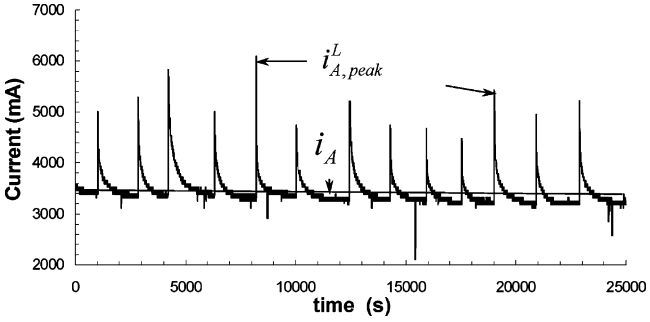

Figure 11. Electrochemical noise in slurry erosion processes.

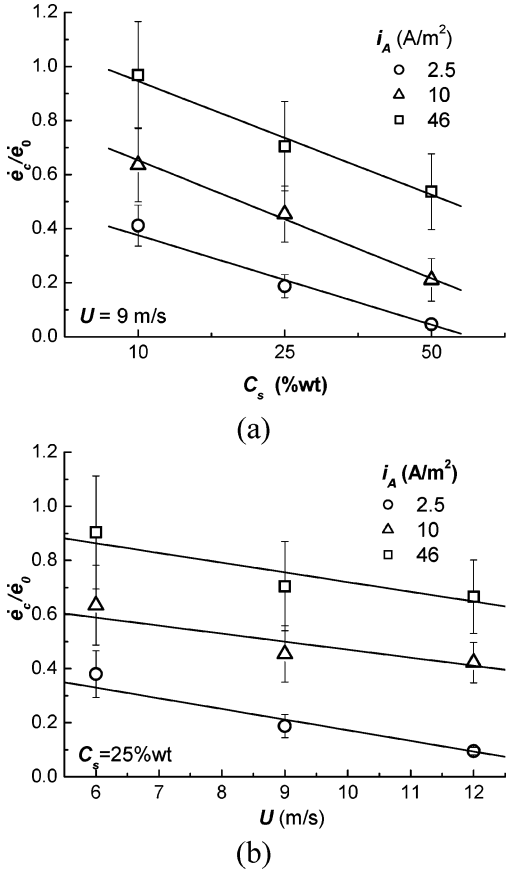

Figure 12. Effects of flow velocity and sand concentration on $\dot{e}_c/\dot{e}_0$.

surface. Hence the chemo−mechanical effect in the slurry-erosion process should be governed by the local current densities over the surface of wear scars rather than the average anodic current density. As a result, the average anodic current density i_A in eq 70 should be replaced by the local anodic current density $i^L_{A,peak}$

$$\frac{\dot{e}_c}{\dot{e}_0} = \frac{nkT}{v_D H v} \log\left(\frac{i^L_{A,peak}}{i_{th}}\right) \tag{72}$$

The physical meanings of $i^L_{A,peak}$ and i_A are schematically shown in Figure 11. Obviously, the difference between $i^L_{A,peak}$ and i_A will decrease with the increase of frequency or width of transient current peaks. According to the data in Figure 12, the normalized corrosion-enhanced erosion rate $\dot{e}_c/\dot{e}_0$ decreases with the sand concentration and flow velocity when the anodic dissolution rate is kept unchanged. This implies that the difference between the actual and predicted values of corrosion-enhanced erosion rate, or the difference between $i^L_{A,peak}$ and i_A,

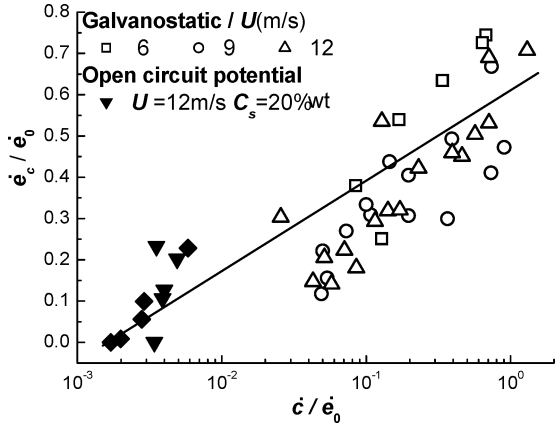

Figure 13. Relationship between $\dot{c}/\dot{e}_0$ and $\dot{e}_c/\dot{e}_0$.

is reduced with increasing frequency of impingements and kinetic energy of sand particles. It is not surprising because the higher sand concentration will cause higher frequency of impingement. In the RCE system used in the current experiments, the impingement angle of sand particle is small, so that the cutting mechanism is likely to dominate the erosion process.[14,15,33] Therefore, the impacts of sand particles with higher kinetic energy will produce wear scars with a larger area and will result in wider transient peaks of current density. In laboratory investigations, there is a practical difficulty in measuring the exact value of $i^L_{A,peak}$ and only the average current density over the electrode surface can be experimentally determined. To evaluate the effect of nonuniform distribution of anodic current, we define

$$q = \frac{i_A}{i^L_{A,peak}} \tag{73}$$

Obviously, $1 \geq q > 0$. The value of q will increase with the sand concentration and flow velocity. Insert eq 73 into eq 72, we have

$$\frac{\dot{e}_c}{\dot{e}_0} = \frac{nkT}{v_D H v} \log\left(\frac{i_A}{q i_{th}}\right) = \frac{nkT}{v_D H v} \log\left(\frac{i_A}{i^L_{th}}\right) \tag{74}$$

Comparing eq 71 with eq 74, the only difference is that i_{th} is replaced by $i_{th}{}^L (= q i_{th})$. The value of i^L_{th} is expected to increase with the intensity of erosion and the latter is enhanced with increasing the sand concentration and flow velocity. When the erosion intensity is sufficiently high the overall surface of the electrode is activated by the impingement of sand particles and it results in $q \rightarrow 1$ and $i^L_{th} \approx i_{th}$. As a first approximation,[29] $q \propto \dot{e}_0$, i.e.,

$$i^L_{th} = \eta \frac{z_M F \dot{e}_0}{M} \tag{75}$$

M is the atomic weight of test material and η an experimental constant. It is known that the weight loss due to electrochemical corrosion can be calculated with the Faraday's secondary law, as indicated by eq 63. Substitute eqs 63 and 75 into eq 74 and we have

$$\frac{\dot{e}_c}{\dot{e}_0} = \frac{nkT}{v_D H v} \log\left(\frac{1}{\eta}\frac{\dot{c}}{\dot{e}_0}\right) = Z \log\left(\frac{\dot{c}}{\dot{e}_0}\right) + C \tag{76}$$

where $Z = nkT/v_D H v$ and $C = -Z \log \eta$. As shown in Figure 13, eq 76 can be approximately used to normalize the effects

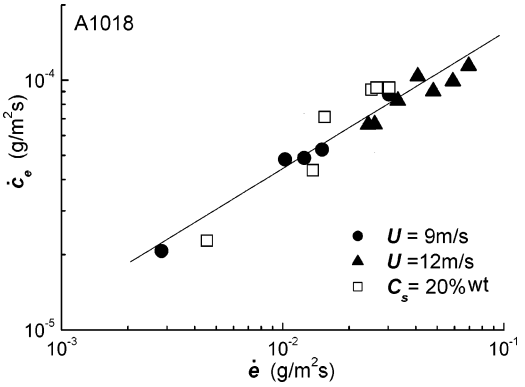

Figure 14. Correlation between $\dot{e}_c$ and $\dot{e}$.

of sand concentration and flow velocity on the corrosion-enhanced erosion rate and, under the current experimental conditions, Z and C can be approximately considered material constants.

Erosion-Enhanced Corrosion. At the open circuit potential, the anodic dissolution current density is equal to the self-corrosion current density. If the corrosion process is controlled by the charge-transfer step, the response of anodic dissolution rate to the dynamically plastic deformation caused by the particle impingement can be formulated with eq 48, so that the self-corrosion current density under slurry-erosion conditions, i_{corr}, can be approximately given as follows:

$$i_{corr} = i_{corr,0} + \frac{z_M F L_{21}}{b\lambda L_{11}}\dot{\gamma}_P^s \tag{77}$$

where $i_{corr,0}$ is the corrosion current density under the condition free of erosion and $\dot{\gamma}_P^s$ is the average surface plastic deformation rate resulting from various mechanical forces in the slurry-erosion process.

According to the definition of erosion-enhanced corrosion, $\Delta i_{corr} = i_{corr} - i_{corr,0}$ is regarded as the increment of corrosion current density caused by erosion

$$\Delta i_{corr} = \frac{z_M F L_{21}}{\bar{b}\lambda L_{11}}\dot{\gamma}_P^s \tag{78}$$

The validity of eq 78 has been experimentally confirmed by the corrosion current density measurement using unnotched tensile specimens.[34,45] At this moment, it is still difficult to formulate the exact relation between the surface plastic deformation rate and the impingement of solid particles because the stress field produced by the particle impingement is rather complicated. However, it is reasonable to expect that the value of $\dot{\gamma}_P^s$ rises with increasing the overall erosion intensity. For a first approximation, we assume that average plastic deformation rate in the surface layer and $\dot{e}$ have the following correlation:

$$\dot{\gamma}_P^s = \kappa_P \dot{e}^{\beta_P} \tag{79}$$

where κ_P and β_P are experimental constants. It is noted that the values of i_{corr} and $i_{corr,0}$ can be, respectively, correlated to $\dot{c}$ and $\dot{c}_0$ with Faraday's secondary law. Inserting eqs 77−79 into eq 3 and using Faraday's secondary law, we have

$$\dot{c}_e = \frac{M}{z_M F}\Delta i_{corr} = \frac{M L_{21}}{b\lambda L_{11}}\dot{\gamma}_P^s = \frac{\kappa_P M L_{21}}{b\lambda L_{11}}\dot{e}^{\beta_P} \tag{80}$$

The applicability of eq 80 has been demonstrated in Figure 14 and the result suggests that $\beta_P \approx 0.5$ give a good approximation. Equation 80 suggests that erosion-enhanced corrosion could be reduced with certain surface strengthening techniques to improve the resistance to the plastic deformation in the surface layer and to suppress the erosion process.

Conclusions

A theoretical model was developed, for the first time, for quantitative predicting the material loss caused by synergism of mechanical and electrochemical factors in erosion−corrosion process, on the basis of the nonequilibrium thermodynamics, electrochemistry, and dislocation kinetics. This model gives a reasonably good prediction for material loss of carbon steel caused by the synergistic effects in slurry erosion. Although more experimental research is needed to check the applicability of this new model, the model analysis will contribute to the comprehensive understanding of the mechanism behind the synergistic effects and to the service life prediction for the slurry pipes on a nonempirical basis. In line with the new model and experimental results, the following conclusions are given:

(1) The synergistic effect in the erosion−corrosion results mainly from the interaction of two irreversible fluxes on the surface suffering erosion−corrosion, namely, the anodic dissolution current density present on the surface and the dislocation flux in the surface layer caused by dynamic plastic deformation. An enhanced anodic dissolution flux is induced by the dynamic surface plastic deformation resulting from the impingement of solid particles; meanwhile, the anodic current present at the electrode surface, in turn, can increase the mobility of dislocation and induces an extra dislocation flux.

(2) The hardness of carbon steel decreases with increasing anodic current density on the surface because of the increase in the dislocation mobility in the surface layer induced by anodic dissolution. The reduced hardness value due to corrosion is a linear function of logarithm of anodic current density and the correlation of relative hardness degradation vs anodic current density is almost independent of the polarization behavior of materials.

(3) The rate of material loss produced by the corrosion-enhanced erosion increases with anodic current density while the pure mechanical erosion rate increases with decreasing hardness, indicating that the hardness degradation caused by the anodic dissolution is a synergistic mechanism in slurry-erosion process.

(4) The normalized corrosion-enhanced erosion rate $\dot{e}_c/\dot{e}_0$ can be expressed as a linear function of logarithm of anodic current density. The effects of sand concentration and flow velocity on the kinetics of corrosion-enhanced erosion can be normalized with the parameter $\dot{c}/\dot{e}_0$, i.e., the ratio of weight losses produced by electrochemical corrosion and mechanical erosion, respectively.

(5) The wastage of erosion-enhanced corrosion may result from the dynamic plastic deformation rate in the surface layer caused by the particle impingement, and in this situation, it is a function of erosion rate.

Acknowledgment. This work was supported by Natural Sciences and Engineering Research Council of Canada.

Nomenclature

A	Real area of impression produced by hardness indentation
A_i	Affinity of irreversible process (i = 1, 2, ...)
$\boldsymbol{A}_P$	Affinity of plastic deformation
$\tilde{A}_M$	Electrochemical affinity of reaction $Me \leftrightarrow Me^{z_M+} + ze^-$

$\tilde{A}_O$	Electrochemical affinity of reaction $O + z_o e^- \leftrightarrow R$
b	Burger vector of dislocation
B_i	State variables of a thermodynamic system ($i = 1, 2, ..., m$)
B_i^0	Value of B_i under the equilibrium state ($i = 1, 2, ..., m$)
$\dot{c}$	Weight loss rate due to corrosion in the presence of erosion
$\dot{c}_0$	Weight loss rate due to corrosion in absence of erosion
$\dot{c}_e$	Weight loss rate due to erosion-enhanced corrosion ($=\dot{c} - \dot{c}_0$)
C_s	Concentration of solid particles in slurry
$\bar{d}$	Average diagonal length of projected Vickers hardness indentation impression
$\dot{e}$	Weight loss rate due to erosion in the presence of corrosion
$\dot{e}_0$	Weight loss rate due to erosion in absence of corrosion
$\dot{e}_c$	Weight loss rate due to corrosion-enhanced erosion ($= \dot{e} - \dot{e}_0$)
e_D, E_D	Potential barrier to be overcome to activate F−R sources ($E_D = N_{max}\, e_D$)
F	The Faraday's constant
F_i	Thermodynamic forces causing irreversible processes ($i = 1, 2, ...$)
g_{ik}	$\partial^2 S/\partial\beta_i\partial\beta_k$, ($i, k = 1, 2, ..., m$)
h	Penetration depth of hardness indentation
Hv	Vickers hardness measured under corrosion-free condition
Hv_c	Vickers hardness measured while anodic current was applied
i_A	Average anodic current density over sample surface
i_{corr}	Self-corrosion current density
$i_{corr,0}$	Self-corrosion current density under conditions free of erosion
Δi_{corr}	Increment of self-corrosion current density caused by erosion ($= i_{corr} - i_{corr,0}$)
i_{th}	Threshold anodic current density to cause the chemo-mechanical effect
$i_{A,peak}^L$	Peak value of local anodic current density over wear scars during sand impingement
i_{th}^L	Equivalent threshold value of i_A^L to cause the chemo-mechanical effect
J_M	Reaction flux of reaction $Me \leftrightarrow Me^{z_M+} + z_M e^-$
J_i	Fluxes of irreversible processes ($i = 1, 2, ...$)
$J_{M,A}$	Irreversible flux of anodic half-reaction of oxidation process $Me \rightarrow Me^{z_M} + z_M e^-$
$J_{M,C}$	Irreversible flux of cathodic half-reaction of oxidation process $Me^{z_M+} + z_M e^- \rightarrow Me$
$J_{O,A}$	Irreversible flux of anodic half-reaction of reduction process $R \rightarrow O + z_o e^-$
$J_{O,C}$	Irreversible flux of cathodic half-reaction of reduction process $O + z_o e^- \leftrightarrow R$
ΔJ_A	Increment of anodic reaction flux on electrode surface induced by erosion
J_M^0	Exchange flux of the oxidation process $Me \leftrightarrow Me^{z_M+} + z_M e^-$
J_O^0	Exchange flux of the reduction process $O + z_o e^- \leftrightarrow R$
J_{th}	Threshold flux of anodic reaction to cause the chemo-mechanical effect
k	Boltzmann's constant
K	A coefficient in relation of P vs h^2 in Vickers hardness measurement
L_{ik}	Phenomenological coefficients in Onsage's reciprocity relations (i, k=1, 2, ...m)
M	Atomic weight of metallic anode
m	Number of irreversible processes in a thermodynamic system
n, n_U, n_H	Exponents in the expressions correlating $\dot{e}_0$ to (U/Hv),U and Hv, respectively
N_A	Avogadro's number
N_{F-R}	Density of dislocation sources
N_{max}	The maximum number of dislocations in a metal with mass of one mole.
$\dot{N}$	Nucleation rate of dislocations or dislocation flux
$\dot{N}^0$	Reversible flux of dislocations
$\dot{N}_A$	Flux of dislocations induced by anodic dissolution
$\dot{N}_P$	Irreversible flux of dislocations
$\dot{N}_P^*$, $\dot{N}_P^{**}$	Irreversible fluxes of dislocations before and after anodic current is applied while overall plastic deformation rate is kept unchanged by adjusting applied stress
p	Probability for activation of a Frank-Read source
P	Indentation load applied during hardness test
P_{max}	Maximum indentation load of hardness test
q	$= i_A/i_{A,peak}^L = i_{th}^L/i_{th}$
r	Radius of cylinder sample
R	The gas constant
R_D	kN_{max}
S	Entropy
$\dot{S}$	Flux of entropy
$\dot{S}_P$	Entropy flux caused by a plastic deformation process
$\dot{S}_{EC}$	Entropy flux caused by an electrochemical process
T	Temperature
U	Apparent flow velocity at the surface of rotating cylinder electrode ($= \omega r$)
$\bar{V}$	Average velocity of dislocation's movement
v_D, V_D	Activation volume of F−R source($V_D = N_{max}\, v_D$)
$\dot{w}$	Total weight loss rate due to erosion-corrosion
$\dot{w}_s$	Weight loss rate due to the synergistic effect ($= \dot{e}_c + \dot{c}_e$)
Y	A coefficient in the expression to correlate Hv and σ_y
Z	A coefficient in the expression correlating $\dot{e}_c/\dot{e}_0$ and log-(i_A/i_{th})
z_M	Number of moles of electrons exchanged in the oxidation process $Me \leftrightarrow Me^{z_M+} + z_M e^-$
z_O	Number of moles of electrons exchanged in the reduction process $O + z_o e^- \leftrightarrow R$
α_M	Charge-transfer coefficient of the oxidation process $Me \leftrightarrow Me^{z_M+} + z_M e^-$
α_O	Charge-transfer coefficient of the reduction process $O + z_o e^- \leftrightarrow R$
β_i	Deviations of state variables under nonequilibrium state ($B_i - B_i^0$)
$\dot{\beta}_i$	Fluxes of irreversible processes
β_P	Exponent in the expression to correlate $\dot{\gamma}_P^s$ and $\dot{c}_e$
γ_P	Plastic shear strain
$\dot{\gamma}_P$	Plastic strain rate
$\dot{\gamma}_P^s$	Plastic deformation rate in surface layer
λ	Mean free path of dislocations
μ_i	Chemical potential (i = 1,2,....)
$\tilde{\mu}_i$	Electrochemical potential (i = 1,2,....)
φ	Electrode potential
φ_0	Equilibrium electrode potential
θ	Open angle of Vickers hardness indenter
$\kappa, \kappa_U, \kappa_H$	Coefficients in the expressions correlating $\dot{e}_0$ to (U/Hv),U and Hv, respectively
κ_P	Coefficient in the expression to correlate $\dot{e}$ to $\dot{\gamma}_P$
σ_{ys}	Tensile yield strength
ν	Vibrational frequency of a F−R source
ν_i	Stoichiometric coefficient

τ	Shear flow stress
τ_i	The athermal component of shear flow stress
τ_{P-N}	The thermal component of shear flow stress (Peierls-Nabarro stress)
τ_{ys}	Shear yield strength
$\tau^*_{P-N}, \tau^{**}_{P-N}$	Peierls-Nabarro stress before and after anodic current is applied while the overall plastic deformation rate is kept unchanged
ΔHv	$= Hv_c - Hv$
$\Delta\tau_A$	Degradation of shear strength due to the presence of anodic dissolution
v	Orientation factor(τ/σ)
ω	Rotating angle speed of cylinder sample

References and Notes

(1) Hutchings, I. M. *The Erosion of Materials By Liquid Flow*, MTI Publication No. 25; Materials Technology Institute of the Chemical Process Industries, Inc.: St. Louis, MO, 1986.

(2) Poulson, B. *Corros. Sci.* **1983**, *23*, 391.

(3) Stack, M. M. *Int. Mater. Rev.* **2005**, *50*, 1.

(4) Christodoulou, P.; Drotlew, A.; Gutowski, W. *Wear* **1997**, *211*, 129.

(5) Pugsley, V. A.; Allen, C. *Wear* **1999**, *233−235*, 93.

(6) Wang, M. C.; Ren, S. Z.; Wang, X. B.; Li, S. Z. *Wear* **1993**, *160*, 259.

(7) Huang, X.; Wu, Y. *J. Mater. Eng. Perform.* **1998**, *7*, 463.

(8) Blatt, W.; Kohloey, W.; Lotz, U.; Heitz, E. *Corrosion* **1989**, *45*, 793.

(9) Bjordal, M.; Bardal, E.; Rogne, T.; Eggen, T. G. *Surf. Coat. Technol.* **1995**, *70*, 215.

(10) Prasad, B. K. *Wear* **2000**, *238*, 151.

(11) Das, S.; Mondal, D. P.; Modi, O. P.; Dasgupta, R. *Wear* **1999**, *231*, 195.

(12) Neville, A.; Hodgkiess, T. *Br. Corros. J.* **1997**, *32*, 197.

(13) Bitter, J. G. A. *Wear* **1963**, *6*, 5.

(14) Finnie, I.; McFadden, D. H. *Wear* **1975**, *48*, 181.

(15) Hutchings, I. M. *Wear* **1981**, *70*, 269.

(16) Sundararajan, G. *Wear* **1991**, *149*, 111.

(17) Lyczkowski, R. W.; Boulliard, J. X. *Prog. Energy Combust. Sci.* **2002**, *28*, 435.

(18) Follansbee, P. S.; Sinclair, G. B.; Williams, J. C. *Wear* **1982**, *74*, 107.

(19) Heitz, E. *Corrosion* **1991**, *47*, 135.

(20) Chen, T. Y.; Moccari, A.; MacDonna, D. D. *The Development of Controlled Hydrodynamic Techniques for Corrosion Testing*, MTI Publication, No. T-3; Materials Technology Institute of the Chemical Process Industries, Inc.: St. Louis, MO, 1992.

(21) Silverman, D. C. *Corrosion* **2004**, *60*, 1003.

(22) Poulson, B. *Wear* **1999**, *233−235*, 497.

(23) Reyes, M.; Neville, A. *J. Mater. Eng. Perform.* **2001**, *10*, 723.

(24) Jiang, X.; Li, S.; Tao, D.; Yang, J. *Corrosion* **1993**, *49*, 836.

(25) Madsen, B. W. *Wear* **1988**, *123*, 127.

(26) Yue, Z.; Zhou, P.; Shi, J. In *Wear of Materials*; Ludema, K. C. Ed.; ASME: New York, 1987; Vol 2, p 763.

(27) Neville, A.; Hu, X. *Wear* **2001**, *250−251*, 1284.

(28) Postlethwaite, J. *Corrosion* **1981**, *37*, 1.

(29) Lu, B. T.; Luo, J. L., Corrosion of Stainless Steels in Flowing Slurries. In *Proc. 16th International Corrosion Congress*; Beijing, China, 2005.

(30) Bester, J. A.; Ball, A. *Wear* **1993**, *162−164*, 57.

(31) Li, Y.; Burstein, G. T.; Hutchings, I. M. *Wear* **1995**, *186−187*, 515.

(32) Matsumura, M.; Oka, Y.; Hiura, H.; Yano, M. *ISIJ Int.* **1991**, *31*, 168.

(33) Endo, S.; Nagae, M. *ISIJ Int.* **1996**, *36*, 87.

(34) Gutman, G. M. *Mechanochemistry of Materials*; Cambridge International Science Publishing: Great Abington, Cambridge, UK, 1998.

(35) Larsen, B. J.; Liang, H. *Wear* **1999**, *233−235*, 647.

(36) Groot, S.; Mazur, P. *Non-Equilibrium Thermodynamics*; Dover Publications: New York, 1984.

(37) Friedel, J. *Dislocations*; Pergamon Press: New York, U.S.A, 1964.

(38) Schock, G., In *Dislocation in Solid;* Nabarro, F. R. N., Ed.; North-Holland Publishing Company: Amsterdam, 1980; p 64.

(39) Li, J. M. C. *Can. J. Phys.* **1967**, *45*, 493.

(40) Lu, B. T.; Zheng, X. L. *Metall. Trans., A* **1992**, *23A*, 2597.

(41) Polak, J.; Klesnil, M. *Mater. Sci. Eng.* **1976**, *26*, 157.

(42) Duquette, D. J. *Corrosion* **1990**, *46*, 434.

(43) Romanov, O. M.; Hencha, B. Ya; Huta, O. M.; Vasulechka, V. O. *Mater. Sci.* **1996**, *32*, 760.

(44) Drazic, D. M.; Gojkoovic, S.; Zecavic, S. K.; Radmilovic, V. *Corros.Sci.* **1992**, *33*, 791.

(45) Raicheff, R. G.; Damajanovic, A.; Bockris, J. O. M. *J. Chem. Phys.* **1967**, *47*, 2198.

(46) Jones, D. A. *Corrosion* **1996**, *52*, 356.

(47) Huang, Y. L. *J. Mater. Sci. Tech.* **2001**, *17*, S77.

(48) Revie, R. W.; Uhlig, H. H. *Acta Metall.* **1974**, *22*, 69.

(49) Gutman, E. M.; Eliezer, A.; Unigovski, Ya; Abramov, E. *Mater. Sci. Eng.* **2001**, *A302*, 63.

(50) Gu, B.; Chu, W. Y.; Qiao, L. J.; Hsiao, C. M. *Corros. Sci.* **1994**, *36*, 1437.

(51) Jones, D. A.; Jankowski, A. F. *Scripta Metall. Mater.* **1993**, *22*, 701.

(52) Seo, M.; Sato, N. *Langmuir* **1987**, *3*, 917.

(53) Lian, K.; Meletis, E. I. *Corrosion* **1996**, *52*, 347.

(54) *Metals Handbook*, Disk Edition; Davis, J. R., Ed.; ASM International: Materials Park, OH, 1998.

(55) Venkatesh, T. A.; Vliet, K. J. V.; Gianakapoulos A. G.; Suesh, S. *Scripta. Mater* **2000**, *42*, 833.

(56) Sakai, M.; Nakano, Y. *J. Mater. Res.* **2002**, *17*, 2161.

(57) Chekrakarty, J. *Theory of Plasticity;* McGraw Hill: New York, 1987.

(58) Nix, W. D.; Gao, H. *J. Mech. Phys. Solids* **1998**, *46*, 411.

(59) Laird, G. II. *Trans. American Foundrymen's Society* **1994**, *102*, 497; **1991**, *99*, 339.

(60) Lu, B. T.; Luo, J. L.; Chiovelli, S. In *Materials Degradation: Innovation, Inspection, Control and Rehabilitation, Proc. 44th Annual Conf. of Metallurgists of CIM;* G. Gu et al. Ed; Calgary, AB, Canada, 2005; p 313.

(61) Guo, H. X.; Lu, B. T.; Luo, J. L. Non-Faraday's Material Loss in Flowing Corrosive Solution, *Electrochim. Acta* **2005,** paper submitted.

(62) Oltra, R.; Chapey, B.; Renaud, L. *Wear* **1995**, *186−187*, 533.

(63) Wood, R. J. K.; Wharton, J. A.; Speyer, A. J.; Tan, K. S. *Tribol. Int.* **2002**, *35*, 631.

(64) Chen, C. W.; Lu, B. T.; Luo, J. L. In *Environmental Degradation of Materials and Corrosion Control in Metals, Proc. 42nd Ann. Conf. Metallurgists of CIM;* Luo, J., Elboujdaini, M., Shoesmith, D. and Patnaik, P. C., Eds.; Vancouver, Canada, 2003; p 43.